transducers designed by these methods probably have very high efficiency-to-length ratios, but mathematical proof of this still is lacking.

It is the purpose of this communication to suggest that the weighting functions are not as arbitrary as they first appear. An additional relationship is imposed by the Kinetic Power Theorem.[3]

In the notation of Solymar and Eaglesfield,[1]

$$\psi_m(x, y, z) = g_1(z)\psi_m{}^A + g_2(z)\psi_m{}^B \quad (1)$$

is a gradually-varying eigenfunction that characterizes signal propagation on the mth transmission line of the tapered transducer. Weighting functions $g_1(z)$ and $g_2(z)$ cause ψ_m to vary from a value of $\psi_m{}^A$ (the eigenfunction of the input mode) at $z=0$, to a value of $\psi_m{}^B$ (the eigenfunction of the output mode) at $z=L$. When ψ_m is constructed in this way, a waveguide cross-sectional boundary can be derived from the orthogonal trajectories of the equipotential contours, as by Solymar and Eaglesfield,[1] or from the normals to the E-field vectors, as by Wolfert.[2] Since the E-field vectors are proportional to the gradients of ψ_m, the two derivations yield the same results. The problem is to find the functions $g_1(z)$ and $g_2(z)$ that optimize the design. This is an extremely complicated mathematical problem for which only empirical approaches have been suggested thus far.

To put the problem in perspective, one may write the following equations relating ψ_m, the scaler magnitude of the Hertzian vector potential, and the field components of a TE-mode propagating on the mth transmission line.

$$\boldsymbol{H}_{tm} = j\beta_m \nabla_t \psi_m e^{-j\beta_m z} \quad (2)$$

$$\boldsymbol{E}_{tm} = j\omega\mu_0 \boldsymbol{k} \times \boldsymbol{H}_{tm} \quad (3)$$

$$H_{zm} = k_{cm}{}^2 \psi_m e^{-j\beta_m z} \quad (4)$$

where β_m and k_{cm} are the propagation and cutoff constants, respectively, of the line, and $\boldsymbol{k}$ is a unit vector on the z axis. It is assumed that β_m and k_{cm} are either constant, or vary sufficiently slowly with z, that hybrid modes are not excited. Actually, this assumption is implied by the separation of variables in (1).

A complex Poynting vector S_m for the mth line can be formed from (2) and (3):

$$S_m = \boldsymbol{E}_{tm} \times \boldsymbol{H}_{tm}{}^* = \omega\mu_0\beta_m(\boldsymbol{k} \times \nabla_t\psi_m) \times \nabla_t\psi_m. \quad (5)$$

Expanding, and integrating over a waveguide cross section $S(z)$, gives the power flowing in the line

$$P_m = \frac{\omega\zeta\beta_m k_{cm}{}^2}{2c} \int_{S(z)} \psi_m{}^2 da \quad (6)$$

where $\zeta = 377\ \Omega$, and c is the velocity of light. If mks units are used, ψ_m is expressed in ampere-meters to yield P in watts.

Although β_m and k_{cm} can be assumed to be invariant from one end of the transducer to the other ($\beta_m{}^A = \beta_m{}^B$, $k_{cm}{}^A = k_{cm}{}^B$) in general, by the nature of its construction, the bounded area S will be a slowly-varying function of z. Nevertheless, for this lossless, reflectionless transducer, the Kinetic Power Theorem requires that

$$\frac{2c}{\omega\zeta\beta_m k_{cm}{}^2}\frac{dP}{dz} = 0 = \frac{d}{dz}\int_{S(z)} [g_1(z)\psi_m{}^A + g_2(z)\psi_m{}^B]^2 da. \quad (7)$$

Eq. 7 provides a relationship between $g_1(z)$ and $g_2(z)$ that depends on the behavior of the boundary. Unfortunately, the equation cannot be integrated without first solving the boundary-value problem, but when the boundary has been derived by the graphical methods discussed in the references, a numerical integration can be carried out to test the validity of the functions. In view of the slowly-varying nature of the cross section, and the fact that $g_1(0)$ and $g_2(L)$ are readily adjusted to equalize the powers in waveguides A and B, it probably is sufficient to carry out the integration at one intermediate cross section, such as at $z=L/2$.

D. B. CHURCHILL
Microwave Engineering Dept. D-40
Sperry Gyroscope Co.
Great Neck, N. Y.

[3] The Kinetic Power Theorem states that any loss in real kinetic power must equal the power delivered externally. It implies a conservation of power flow through a lossless, reflectionless transducer.

On the Focused Fabry-Perot Resonator in Plasma Diagnostics

In a recent paper, Primich and Hayami[1] discussed the application of a Fabry-Perot resonator to plasma diagnostics. In particular, they studied plasma densities that are uniform in space and that have a plasma frequency much less than the operating frequency of the microwave system. They also restrict themselves to plasmas that are collisionless.

The purpose of this communication is to study the use of a Fabry-Perot resonator in diagnostics of a low density but nonuniform plasma and also to consider the plasma to have collisions. Such a problem would arise in determining the plasma parameters in the wake of a projectile or in various low density plasma confinement devices.

Consider the resonator shown in Fig. 1 with a plasma slab inserted in it. One can consider plane waves[2,3] to be propagating in the resonator, hence the plasma slab may be considered as a dielectric medium of dielectric constant ϵ_{p1}.

$$\epsilon_{p1} = \epsilon_0\left[1 - \frac{\omega_p{}^2}{\omega^2 - j\omega\nu}\right] \quad (1)$$

Manuscript received April 27, 1964.

[1] R. I. Primich and R. A. Hayami, "The application of the focused Fabry-Perot resonator to plasma diagnostics," IEEE TRANS. ON MICROWAVE THEORY AND TECHNIQUES, vol. MTT-12, pp. 33–42; January, 1964.
[2] G. Goubau and F. Schwering, "On the guided propagation of electromagnetic wave beams," IRE TRANS. ON ANTENNAS AND PROPAGATION, vol. AP-9, pp. 248–256; May, 1961.
[3] W. Culshaw, "Further considerations on Fabry-Perot type resonators," IRE TRANS. ON MICROWAVE THEORY AND TECHNIQUES, vol. MTT-10, pp. 331–339, September, 1962.

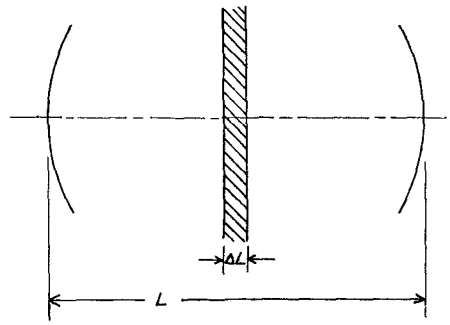

Fig. 1—Fabry-Perot plasma diagnostic device.

where $\omega_p{}^2 = ne^2/m\epsilon_0$ is the plasma frequency and ν is the collision frequency. For $\nu \ll \omega$, (1) becomes

$$\epsilon_{p1} \approx \epsilon_0\left[1 - \frac{\omega_p{}^2}{\omega^2} + j\frac{\omega_p{}^2\nu}{\omega^3}\right]. \quad (2)$$

Consider now the Fabry-Perot cavity to be resonated in the absence of any plasma medium. Finite losses are present resulting from the reflecting end plates and diffraction, hence the complex resonant frequency is expressible as

$$\Omega_0 = \omega_0\left[1 + \frac{j}{2Q_0}\right] \quad (3)$$

where ω_0 is the natural resonant frequency and Q_0 is the Q of the empty cavity. Introduction of the plasma slab will cause the resonant frequency to shift by an amount $\delta\omega$; hence the new complex resonant frequency may be written as

$$\Omega_1 = (\omega_0 + \delta\omega)\left[1 + \frac{j}{2Q_1}\right]. \quad (4)$$

As the Q's of the Fabry-Perot cavity are very high, one obtains

$$\frac{\Omega_1 - \Omega_0}{\omega_0} \approx \frac{\delta\omega}{\omega_0} + \frac{j}{2}\left[\frac{1}{Q_1} - \frac{1}{Q_0}\right]. \quad (5)$$

The fields before and after the introduction of the plasma slab will be relatively unchanged as $\epsilon_{p1} \approx \epsilon_0$, hence the use of the perturbational concept[4] is valid which yields

$$\frac{\Omega_1 - \Omega_0}{\Omega_0} = \frac{-\iiint_{\Delta V}(|\Delta\epsilon|\,|E_0|^2 + \Delta\mu\,|H_0|^2)dV}{\iiint_V(\epsilon_0|E_0|^2 + \mu_0|H_0|^2)dV} \quad (6)$$

where in general Ω, μ, and ϵ are complex. At resonance, the electric and magnetic energies are equal and the plasma does not alter the permeability, hence (6), using (2) and (5) becomes

$$\frac{\Omega_1 - \Omega_0}{\omega_0} = \frac{\iiint_{\Delta V}\left[\frac{\omega_p{}^2}{\omega_0{}^2} - j\frac{\omega_p{}^2\nu}{\omega_0{}^3}\right]|E_0|^2 dV}{2\iiint|E_0|^2 dV} = \frac{\delta\omega}{\omega_0} + \frac{j}{2}\left[\frac{1}{Q_1} - \frac{1}{Q_0}\right]. \quad (7)$$

[4] R. F. Harrington, "Time-Harmonic Electromagnetic Fields," McGraw-Hill Book Co., Inc., New York, N. Y., pp. 317–380; 1961.

Equating the real and the imaginary parts of (7) results in

$$\frac{2\delta f}{f_0} = \frac{\iiint_{\Delta V} \frac{\omega_p^2}{\omega_0^2} |E_0|^2 dV}{\iiint_V |E_0|^2 dV} \quad (8)$$

and

$$\frac{Q_0 - Q_1}{Q_0 Q_1} = \frac{\iiint_{\Delta V} \frac{\omega_p^2 \nu}{\omega_0^3} |E_0|^2 dV}{\iiint_V |E_0|^2 dV}. \quad (9)$$

Eqs. (8) and (9) are the most general results as they allow for a density variation, hence also a collision frequency variation, both in the transverse and in the longitudinal directions. One could now perform these integrations using an assumed spatial distribution in both the transverse and longitudinal directions.

As an example, consider a uniform density plasma slab of infinite cross section placed in the resonator. One obtains upon integrating (8) and (9)

$$\frac{2\Delta f}{f_0} = \frac{\Delta L}{L} \frac{\omega_p^2}{\omega_0^2} \quad (10)$$

$$\frac{Q_0 - Q_1}{Q_0 Q_1} = -\frac{\Delta L}{L} \frac{\omega_p^2 \nu}{\omega_0^3}. \quad (11)$$

Using the measured change in resonant frequency, (10) may now be solved for the number density. Using the measured change in the cavity Q, (11) will yield the collision frequency. Eq. (10) is identical to (8) of Primich and Hayami with ΔN replaced by $-\omega_p^2/2\omega^2$ which is shown later in their text.

Experimental comparison with Langmuir probe measurements made in a toroidal octupole plasma confinement device[5] verify the above theory. At 10 Gc the resonator measured a number density of 5×10^9 el/cm^3 as also did the probe.

The parameters Δf and f_0 can be measured to a greater precision using a dual mode[6] cavity. The ratio $\Delta f/f_0$ has been measured as 3×10^{-8} at 35 Gc, hence the diagnostic capability in this frequency range would be to measure number densities from 10^6 el/cm^3 to 10^{14} el/cm^3.

The collision frequency relation (9) could alternatively be derived by considering the transmission line analog of a resonant cavity, solving for the attenuation constant which would depend on the collision frequency of such a line, relating it to the Q's of the filled and unfilled cavities, and finally solving for the collision frequency.

K. E. Lonngren
J. W. Mink
J. B. Beyer
Dept. of Elec. Engrg.
University of Wisconsin
Madison, Wis.

[5] W. E. Wilson and D. M. Meade, "Langmuir probe measurements on plasma in a torroidal octupole magnetic field," *Bull. Am. Phys. Soc.*, to be published.
[6] E. H. Scheibe, "Surface Wave and Antenna Engineering Research Study," University of Wisconsin, Madison, Tenth Quarterly Progress Rept., Contract No. DA-36-039-sc-85188; March 31, 1964.

Step-Twist Diode Switch

Two X-band diode switches have been combined with a step-twist waveguide section to form a very compact broad-band step-twist diode switch.

The device shown in Fig. 1 can replace a step twist in a system when it is necessary to add a switch to the system.

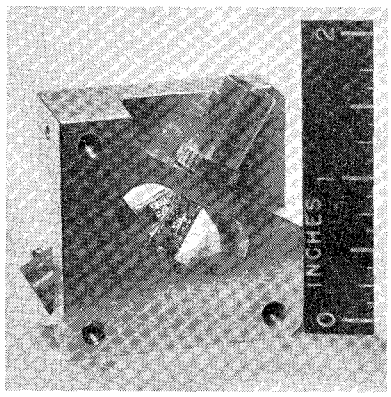

Fig. 1—Step-twist diode switch.

The step twist consists of equal length equiangular twisted sections cut quite inexpensively with a 0.400 inch diameter mill. The VSWR of the step twist alone is shown in Fig. 2.

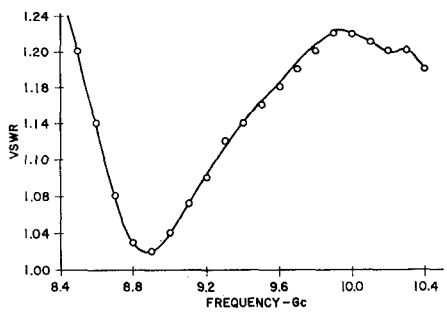

Fig. 2—Step-twist characteristics.

The diode switch consists of two 1N263 diodes centered in each step. The switching voltage is delivered to the diodes through modified BNC connectors. The isolation of two diode switches is a maximum when they are about a quarter wavelength apart. These diodes are a quarter wavelength apart at 10.2 Gc but a capacitive step separates them, lowering the frequency slightly. From Fig. 3 it can be seen that the isolation is greater than 40 db from 8.4 Gc to 10.4 Gc peaking at 9.9 Gc. The insertion loss is less than 3 db from 9.2 Gc to 10.4 Gc. Although the diodes used are limited to switching powers below 50 mw, any of the wide selection of higher power X-band diode switches could be used in this structure.

Manuscript received April 27, 1964.

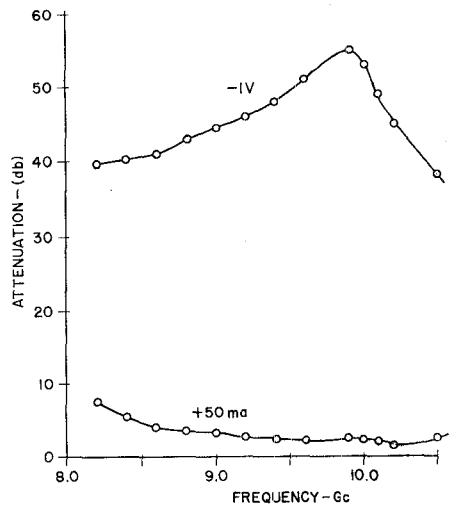

Fig. 3—Frequency dependence of the isolation and insertion loss of the step-twist diode switch.

H. S. Jones, Jr.
R. V. Garver
Harry Diamond Labs.
Washington, D. C.

Dielectric Resonators for Microwave Applications

The purpose of this communication is to report certain test results recently obtained with resonators made of single crystal rutile. Since rutile has a very high dielectric constant and a very low loss factor, microwave resonators made of rutile have several desirable characteristics. Compared to metallic resonators it is possible to reduce the size of the rutile resonator, which is especially useful at lower microwave frequencies. The Q factor of rutile resonators is very high and at room temperature may be of the order of several thousand, while at liquid helium temperature it may even reach 10^5. It can be shown that the ratio of electric and magnetic field strengths of dielectric cavity to metallic cavity is proportional to $(E)^{1/4}$ and $(E)^{3/4}$, respectively. Therefore, with the same available power, an increase in field intensity can be obtained. Furthermore, these fields are not confined to the inside of the rutile resonator but extend beyond the dielectric surface into free space. Because of these characteristics rutile resonators are finding useful applications in traveling-wave masers, in harmonic generators (in conjunction with varactor diodes), in novel RF Hall-effect-devices, and in experiments with parametric superconducting devices.

Manuscript received May 4, 1964. The research reported in this paper was sponsored by the Air Force Cambridge Labs., Office of Aerospace Research, under Contract No. AF19(628)-262, and RCA Labs., Princeton, N. J.